Atomistic Model of Diopside–K-jadeite ($CaMgSi_2O_6$–$KAlSi_2O_6$) Solid Solution

V. L. Vinograd[a], O. G. Safonov[b], D. J. Wilson[a], L. L. Perchuk[b,†], L. Bindi[c], J. D. Gale[d], and B. Winkler[a]

[a]University of Frankfurt, Institute of Geosciences, Altenhöferallee 1, 60054 Frankfurt a.M., Germany
e-mail: V.Vinograd@kristall.uni-frankfurt.de

[b]Institute of Experimental Mineralogy, Russian Academy of Science,
ul. Institutskaya 4, Chernogolovka, Moscow oblast, 142432 Russia
e-mail: oleg@iem.ac.ru

[c]Museo di Storia Naturale, sezione di Mineralogia, Universitá degli Studi di Firenze,
Via La Pira, 4, I-50121, Firenze, Italy
e-mail: luca.bindi@unifi.it

[d]Nanochemistry Research Institute, Department of Applied Chemistry, Curtin University of Technology,
PO Box U1987, Perth 6845, Western Australia
e-mail: julian@ivec.org

Received January 11, 2010

Abstract—Atomistic model was proposed to describe the thermodynamics of mixing in the diopside–K-jadeite solid solution ($CaMgSi_2O6$–$KAlSi_2O_6$). The simulations were based on minimization of the lattice energies of 800 structures within a $2 \times 2 \times 4$ supercell of $C2/c$ diopside with the compositions between $CaMgSi_2O_6$ and $KAlSi_2O_6$ and with variable degrees of order/disorder in the arrangement of Ca/K cations in M2 site and Mg/Al in M1 site. The energy minimization was performed with the help of a force-field model. The results of the calculations were used to define a generalized Ising model, which included 37 pair interaction parameters. Isotherms of the enthalpy of mixing within the range of 273–2023 K were calculated with a Monte Carlo algorithm, while the Gibbs free energies of mixing were obtained by thermodynamic integration of the enthalpies of mixing. The calculated $T–X$ diagram for the system $CaMgSi_2O_6$–$KAlSi_2O_6$ at temperatures below 1000 K shows several miscibility gaps, which are separated by intervals of stability of intermediate ordered compounds. At temperatures above 1000 K a homogeneous solid solution is formed. The standard thermodynamic properties of K-jadeite ($KAlSi_2O_6$) evaluated from quantum mechanical calculations were used to determine location of several mineral reactions with the participation of the diopside–K-jadeite solid solution. The results of the simulations suggest that the low content of $KalSi_2O_6$ in natural clinopyroxenes is not related to crystal chemical factors preventing isomorphism, but is determined by relatively high standard enthalpy of this end member.

DOI: 10.1134/S0869591110040089

INTRODUCTION

Clinopyroxenes in typical crustal rocks formed at comparatively low pressures contain only trace amounts of K_2O, because large potassium ion under these conditions is much more easily accommodated by the lattices of framework and sheet silicates. At the same time, clinopyroxene from mantle xenoliths in kimberlites and lamproites (Bishop et al., 1978; Reid et al., 1976; Jaques et al., 1990) as well as clinopyroxene inclusions in diamonds often contain up to 0.2 wt % K_2O, reaching up to 1.4–1.7 wt % in individual

---

[†] Deceased.

Mineral abbreviations: *Coe*—coesite, *Cpx*—clinopyroxene, *Di*—diopside, *Grs*—grossular, *Hol*—hollandite-structured $KAlSi_3O_8$, *Jd*—jadeite, K-*Cpx*—potassium-bearing clinopyroxene, K-*Jd*—potassium jadeite, *Ks*—kalsilite, *Ky*—kyanite, *Lc*—leucite, *Mic*—microcline, *Prp*—pyrope, *Qtz*—quartz, *San*—sanidine, *Sti*—stishovite, Si-*Wd*—Si-wadeite.

samples (Prinz et al., 1975; Meyer, 1987; Ricard et al., 1989; Harlow and Veblen, 1991; Stachel et al., 2000). K-rich clinopyroxenes with K_2O contents up to 1.0–1.5 wt % (occasionally, up to 3.6 wt %, Bindi et al., 2003) were noted also in the garnet–clinopyroxene silicate and carbonate–silicate rocks of the Kokchetav Complex, Northern Kazakhstan (Sobolev and Shatsky, 1990; Perchuk et al., 2002, 2003; Korsakov and Hermann, 2006). Clinopyroxene phenocrysts with more than 2 wt % K_2O were also found in the potassic hawaiites of West Australia (Ghorbani and Middlemost, 2000). Findings of these samples indicate that clinopyroxene lattice at high pressures is capable to retain sufficiently large amounts of K_2O.

This conclusion is also confirmed by experimental studies. The works of Harlow (1997, 1999) and Chudinovskikh et al. (2001), as well as our experiments (Safonov et al., 2003, 2004, 2005, 2006) showed that

Table 1. Unit cell parameters of microcline (space group $P\bar{1}$) and quartz (space group $P3_221$) calculated with the empirical potentials method (EPM) and density functional theory (DFT GGA) as compared to the experimental data (EXP)

Unit cell parameter	Microcline			α-quartz		
	EXP[a]	EPM	DFT	EXP[b]	EPM	DFT
a (Å)	7.921	7.928	8.008	4.916	4.947	5.058
b (Å)	7.612	7.663	7.687	4.916	4.947	5.058
c (Å)	7.212	7.221	7.304	5.405	5.434	5.543
α (degrees)	76.55	76.702	76.572	90.00	90.00	90.00
β (degrees)	104.38	104.925	104.308	90.00	90.00	90.00
γ (degrees)	66.87	67.118	67.238	120.00	120.00	120.00
Volume (Å³)	360.56	362.674	373.719	113.131	115.176	122.820

Note: The experimental data were taken from the works: [a] (Finney and Bailey, 1964), [b] (Levien et al., 1980).

clinopyroxenes in equilibrium with K-silicate or carbonate–silicate systems at pressures of 6–11 GPa may contain up to 4.0–5.7 wt % K_2O. It was shown the enrichment of clinopyroxene in potassium is primarily caused by the composition of crystallization environment, being thus the indicator of not only the pressure but also the activity of potassium in fluids and melts of mantle origin (Perchuk et al., 2002; Safonov et al., 2005).

The partitioning of $KAlSi_2O_6$ between K-*Cpx* and potassic aluminosilicate melt was experimentally calibrated and applied for estimating the pressure for K-*Cpx*–melt assemblage from inclusions in diamonds and eclogite nodules in kimberlites (Perchuk et al., 2002; Safonov et al., 2005). However, as for K-*Cpx* ⇌ melt equilibrium, the equilibria of K-bearing clinopyroxene with $KAlSi_3O_8$ polymorphs (sanidine, hollandite), phlogopite, or phengite also could serve as efficient geobarometers. The corresponding equations can be obtained using both standard thermodynamic properties of K-*Jd*, and activity of this component in the K-*Cpx* solid solution. However, the calculation of the standard thermodynamic properties and the functions of mixing solely on the basis of experimental data is problematic, because of the limited range of experimentally accessible K-*Jd* concentrations. The experimental study of the $CaMgSi_2O_6$–$KAlSi_2O_6$ system, the model system for the K-*Cpx* solid solution (Safonov et al., 2003), showed that K-*Jd* content in the synthetic clinopyroxenes at 7 GPa does not exceed 26 mol %. The compositions with higher K content are broken down into pyrope–grossular garnet and Si-wadeite according to reaction 4K-*Jd* + 3*Di* = *Grs* + *Prp* + 2Si-*Wd*.

In this study, the standard thermodynamic properties of K-*Jd* were estimated for the first time on the basis of ab initio and force-field, modeling. A force-field model was also used for calculating thermodynamic properties of mixing in the diopside–K-jadeite solid solution following the approach, of Vinograd et al. (2007a).

COMPUTER SIMULATIONS

Calculations Based on Empirical Interatomic Potentials

The structural and thermodynamic properties of K-jadeite could be calculated using a set of transferable empirical interatomic potentials, i.e., parametric functions, which simulate the energy of atomic interaction as functions of interatomic distances. These potentials can be obtained by fitting to the properties of well studied compounds of similar composition and structure. The functional forms of the potentials were taken from the studies of Sanders et al., 1984; Catlow, 1988, Patel et al., 1991; Winkler et al., 1991. The electrostatic interaction between particles was described assuming formal charges on cations and anions, while short-range repulsive forces were simulated by Buckingham potentials. The model also includes three-body interactions, where potential energy depends on O-M-O angle formed by cation (M) and adjacent oxygen atoms (O), as well as shell-core interaction, which enables description of polarizability of large anions (oxygen). The set of potentials for Na, Ca, Mg, Al, Si, and O was successfully tested in the studies of Vinograd et al., 2007a , where it has been shown that phase transitions in omphacite ($CaNaMgAlSi_4O_{12}$) and cordierite ($Mg_3Al_4Si_5O_{18}$) can be simulated in good agreement with available experimental data. The Buckingham K–O potential (A = 1842.52 eV, ρ = 0.289916 Å) has been developed using the relax-fitting procedure (Gale, 1996, 1998) built in the GULP package (General Utility Lattice Program; Gale, 1997; Gale and Rohl, 2003). The obtained parameters were fitted to the data on kalsilite (Cellai et al., 1999), Si-wadeite (Swanson and Prewitt, 1983) and ordered

Table 2. Unit cell parameters and the excess enthalpies of diopside, K-Jd and the intermediate compounds A$_1$, A$_2$, and C$_1$ calculated with the empirical potentials method (EPM) and with density functional theory (DFT)

Unit cell parameter	CaMgSi$_2$O$_6$ ($C2/c$)			C$_1$: Ca$_2$Mg$_2$KAlSi$_6$O$_{18}$ ($B2/n$)	
	EXP*	EPM	DFT	EPM	DFT
a (Å)	9.747	9.750	9.919	16.156	16.306
b (Å)	8.924	8.928	9.065	9.630	9.764
c (Å)	5.252	5.277	5.339	8.882	9.045
α (degrees)	90.00	90.00	90.00	90.00	90.00
β (degrees)	105.94	106.13	106.60	90.00	90.00
γ (degrees)	90.00	90.00	90.00	70.783	70.369
Volume (Å^3)	439.28	441.30	460.03	1304.89	1356.33
ΔH_{mix}, kJ/mol	0	0	0	−2.84	−3.10
$X_{K\text{-}Jd}$	0			0.33	

Unit cell parameter	A$_2$: CaMgKAlSi$_4$O$_{12}$ $P2/n$, normal omphacite			A$_1$: CaMgKAlSi$_4$O$_{12}$ $P2/n$, inverted omphacite		KAlSi$_2$O$_6$ ($C2/c$)	
	EXP*	EPM	DFT	EPM	DFT	EPM	DFT
a (Å)	9.585	9.6078	9.747	9.613	9.749	9.556	9.667
b (Å)	8.776	8.856	8.990	8.845	9.039	8.750	8.896
c (Å)	5.260	5.321	5.357	5.298	5.322	5.319	5.334
α (degrees)	90.00	90.00	90.00	90.00	90.00	90.00	90.00
β (degrees)	106.8	107.27	106.96	106.11	105.88	107.06	105.81
γ (degrees)	90.00	90.00	90.00	90.00	90.00	90.00	90.00
Volume (Å^3)	425.45	432.36	448.96	432.79	451.13	425.19	441.32
ΔH_{mix}, kJ/mol		−1.59	1.11	−3.97	−5.17	0	0
$X_{K\text{-}Jd}$	0.5			0.5		1	

Notes: The values of ΔH_{mix} are given per formula unit of pyroxene with one SiO$_3$ group. The results of calculations for diopside $C2/c$ were taken from the work (Vinograd et al., 2007a). *The experimental data are for synthetic diopside (Raudsepp et al., 1990) and for natural omphacite (Matsumoto et al., 1975).

low-temperature microcline $P\bar{1}$ (Finney and Bailey, 1964; Hearmon, 1984). $P\bar{1}$ structure was used instead of $C\bar{1}$, as the non-standard $C\bar{1}$ cannot be used with GULP.

Table 1 shows the predicted and experimentally measured unit-cell parameters of microcline and α-quartz, while Table 2 reports the unit-cell parameters of diopside, K-jadeite, and three ordered compounds, A$_1$, A$_2$, and C$_1$, calculated using empirical interatomic potentials. The compounds A$_1$ and A$_2$ have the $Di_{50}KJd_{50}$ composition (i.e. K$_2$Al$_2$Ca$_2$Mg$_2$Si$_8$O$_{24}$) and the space group $P2/n$ of omphacite. The cation arrangement in phase A$_2$ is similar to that in omphacite, with Na replaced by K. The position of K and Ca in the phase A$_1$ is inverted with respect to A$_2$ structure. Compound C$_1$ has the space group $B2/n$ and the composition of 2/3 diopside and 1/3 jadeite (K$_4$Al$_4$Ca$_8$Mg$_8$Si$_{24}$O$_{72}$). The relevance of these compounds in the studied system will be explained below.

Quantum−Mechanical Calculations

The structures of α-quartz, microcline, diopside, K-jadeite, and A$_1$, A$_2$, and C$_1$ compounds were calculated using the CASTEP code (Clark et al., 2005) based on density functional theory (DFT; Hohenberg and Kohn, 1964). The computational scheme included expansion of the charge density in the plane wave basis set and the use of "ulrasoft" pseudopotentials (Vanderbilt, 1990; Kresse and Hafner, 1994). The electron−electron exchange and correlation interactions were treated in the framework of the generalized gradient approximation according to PBE model (Perdew et al., 1996). The calculations were performed using primitive unit cells. The k-space integration in the Brillouin zone was performed using Monkhorst-Pack grids ($10 \times 10 \times 8$ for quartz; $6 \times 6 \times 6$ for microcline; $6 \times 6 \times 8$ for K-jadeite and diopside; $4 \times 4 \times 4$ for phase C$_1$; and $6 \times 4 \times 8$ for phases A$_1$ and A$_2$). These grids give approximately the same spacing of about 0.025 Å^{-1} between neighboring points. The structures of diopside and K-jadeite were also calcu-

Table 3. The estimated standard (298 K and 1 bar) thermodynamic properties of K-jadeite, K-omphacite and the phase C_1

Phase	ΔH^f_{298}, kJ/mol	S_{298}, J/K/mol	V_{298}, J/bar/mol	$\alpha \times 10^{-5}$, K^{-1}
$KAlSi_2O_6$ (K-*Jd*)	−2932.7	141.24	6.479	3.3 (298−1298 K)
$(MgCaKAlSi_4O_{12})/2$ (K- omphacite; A_1)	−3077.95	141.22	6.556	3.2 (298−1298 K)
$(Mg_2Ca_2KAlSi_6O_{18})/3$ (C_1)	−3118.79	142.0	6.547	3.3 (298−1298 K)

lated at elevated pressures. The unit-cell parameters calculated ab initio were compared to those predicted on the basis of empirical potentials in Tables 1 and 2. The ab initio calculations indicate systematically large unit-cell parameters (by 1−3%), which is a typical result of the PBE model. Table 2 also lists excess energies of A_1, A_2, and C_1 compounds calculated ab initio and using method of empirical potentials. The comparison of these values demonstrates that this method predicts well the relative energies of these compounds. The energy of A_2 compound is slightly underestimated. We suggest however that this inaccuracy cannot significantly affect the further modeling results, because the A_2 phase is metastable relative to A_1 (see below).

ESTIMATION OF THE THERMODYNAMIC PROPERTIES OF K-JADEITE

The energies and volumes of α-quartz, microcline, and K-jadeite calculated ab initio make it possible to estimate the enthalpy $\Delta H_{(1)}$ and volume $\Delta V_{(1)}$ effects of the reaction

$$K\text{-}Jd + \alpha\text{-}Qtz = Mic. \qquad (1)$$

Obtained values $\Delta H_{(1)} = -131.5$ kJ/mol and $\Delta V_{(1)} = 21.44$ cm³/mol in combination with the standard enthalpies of formation and the standard volumes of microcline and α-quartz (ΔH^f_{298} and V_{298}) tabulated in the data base of Holland and Powell (1998) were used to calculate the corresponding standard properties of

Table 4. The dependence of unit-cell volumes of diopside and K-jadeite on pressure as calculated from density functional theory

Pressure, GPa	V, Å³		ΔV, Å³
	diopside	K-jadeite	
0	460.03	441.32	18.71
2	450.55	434.56	15.99
4	441.93	428.16	13.77
6	434.53	422.29	12.24
8	427.97	416.81	11.16
10	421.90	411.59	10.31

K-jadeite. For instance, the standard enthalpy was calculated using equation ΔH^f_{298} (K-*Jd*) $= \Delta H_{(1)} - \Delta H^f_{298}$ (*Mic*) $+ \Delta H^f_{298}$ (α-*Qtz*) (Table 3). The standard enthalpy of K-omphacite (the phase A_1) was estimated by adding the excess energy of the phase (Table 2) to the half-sum of the standard enthalpies of diopside and K-jadeite. The enthalpy of diopside was taken from data base of Holland and Powell. The standard enthalpy of phase C_1 was obtained by addition of the corresponding value from Table 2 to the sum of standard enthalpies of diopside and K-jadeite in proportions 1/2 and 1/3, respectively. The standard volumes of phases A_1 and C_1 were derived using volume effect of reaction (1) by analogy with the calculation of standard enthalpies.

The P–V data for K-jadeite and diopside (Table 4) calculated ab initio were obtained by fitting to the second-order Birch-Murnaghan equation. The calculated bulk modulus of diopside (97 GPa) is 13% less than experimental value (112 GPa, Aleksandrov et al., 1964). Underestimation of bulk modulus by 10−15% is a typical result of generalized gradient approximation (GGA) (e.g., Ono et al., 2008). Therefore, we suggest that our value of 124.5 GPa for jadeite is also underestimated and that the real bulk modulus of this end member should be close to 145 GPa. The higher bulk modulus of K-jadeite is in qualitative agreement with the experimental results of 129 GPa (Bindi et al., 2006) for a K-*Cpx* crystal with 12 mol % K-*Jd*, which shows that the bulk modulus of K-*Cpx* increases with the K content. The higher bulk modulus also corresponds to the lower standard volume of K-jadeite with respect to diopside (calculated values are 441.32 Å³ for K-jadeite vs. 460.03 Å³ for diopside). Actually, the measurements of Bindi et al. (2006) showed that the volume of K-*Cpx* with 12 mol % K-*Jd* (435.49 Å³) is lower than the volume of pure diopside (439.28 Å³). The lower unit cell volumes relative to diopside were also measured for two K-*Cpx* crystals synthesized in the join $CaMgSi_2O_6$–$KAlSi_3O_8$ at 6 GPa (Safonov et al., 2005, p. 325). These data confirm the trend of decreasing K-*Cpx* volume with growth of K-*Jd*. However, the X-ray single-crystal diffraction data for crystal containing 23 mol % of K-*Jd* (Bindi et al., 2002) show a different tendency: 446.29 Å³ vs. 439.28 Å³ at 23 and 0 mol % of K-*Jd*, respectively. The anomalously

high volume of this clinopyroxene needs further investigations.

The temperature-dependent standard properties of K-jadeite were calculated using the method of lattice dynamics within the quasi-harmonic approximation using ZSISA model (Zero Static Internal Stress Approximation; Allan et al., 1996) built in GULP (Gale, 1997). The standard entropy of K-jadeite is 144.5 J/K/mol, whereas those of jadeite and diopside are 136.8 and 145.1 J/K/mol, respectively. Two latter values are close to the values of 133.5 and 142.7 J/K/mol tabulated for jadeite and diopside by Holland and Powell (1998). The mismatch of 3.3 and 2.4 J/K/mol between estimated and tabulated values of entropies suggests that the applied model of empirical potentials slightly overestimates the standard entropy of K-jadeite, as well as A_1 and A_2 compounds. Therefore, our estimates of the standard entropy of these compounds presented in Table 3 are 3.3 J/K/mol are lower than values predicted from the lattice dynamics calculations. Our calculations suggest that the thermal expansion coefficient of K-Jd (2.73×10^{-5} K^{-1}) in a temperature range of 298–1298 K is slightly higher than the corresponding value of jadeite (2.2×10^{-5} K^{-1}) and diopside (2.65×10^{-5} K^{-1}). The tabulated values for the thermal expansion coefficients of jadeite and diopside are 2.47×10^{-5} K^{-1} and 3.3×10^{-5} K^{-1}, respectively (Cameron et al., 1973), which is approximately 20% higher than values calculated by us. Therefore, our estimates of thermal expansion coefficients of K-jadeite and K-omphacite (Table 3) are 1.2 times higher than values obtained by the lattice dynamics calculations. The heat capacities also could be obtained using lattice dynamics method. However, since anharmonic effects at high temperatures could not be taken into account in quasi-harmonic approximation, further calculations were based on the assumption that the high-temperature heat capacity of K-jadeite is similar to that of diopside. The similar values of standard volumes and thermal expansion coefficients for K-jadeite and diopside support this assumption.

Simulation of Mixing Properties

The thermodynamic mixing properties of the Di–K-Jd solid solution were calculated using the supercell method (Becker et al., 2000; Bosenick et al., 2000, 2001; Warren et al., 2001; Becker and Pollock, 2002; Lavrentiev et al., 2006; Vinograd and Sluiter, 2006; Vinograd et al., 2006, 2007a, 2007b; Palin and Harrison, 2007). This method enables evaluation of the thermodynamic mixing functions by weighting the contributions of a large number of configurations (microstates) within a reasonably large supercell according to the Boltzmann distribution law. Since thermodynamically meaningful results could be obtained only with supercells containing thousands of the exchangeable atoms, the calculation of the weight factors implies a possibility of being able to calculate the energies of individual configurations fast. This problem is solved using method of "cluster expansion" (Connolly and Williams, 1983; Sanchez et al., 1984), which allows evaluation of the excess energy of any solution as a sum of contributions from various clusters of different shape and size. The cluster is referred to as a set of locally defined lattice points of certain geometric shape. Since such a summation requires little time, the average values can be calculated with a Monte Carlo algorithm. The cluster can be visualized as a pair of lattice points located at a given distance from each other. A typical cluster expansion includes all geometrically different pairs of super-cell clusters. A rapid decrease of energies of inter-atomic interactions with increasing distance between atoms makes it possible to exclude pairs located at distances more than 10 Å (Becker et al., 2000; Bosenick et al., 2001) and to determine the effective energies of clusters by considering the reasonably compact supercell. In this work, we used a $2 \times 2 \times 4$ supercell of $C2/c$ diopside containing 128 exchangeable atoms and 37 geometrically different pairs within the range of 3–9 Å. The excess enthalpy was calculated using the equation:

$$H_i = \sum_n f_{AB}^{(n)} J_n + H_0, \qquad (1)$$

where $f_{AB}^{(n)}$ are the numbers of AB-type pairs per super-cell at the nth distance and J_n is the effective pairwise interaction at the nth distance, which is equal to the enthalpy of the exchange reaction AA + BB = 2AB between pairs of A (Ca or Mg) and B (K or Al) atoms located at the nth distance. H_0 is a configuration-independent term, whose compositional dependence is modeled with the equation:

$$H_0 = x_1 x_2 (x_1 A_1 + x_2 A_2), \qquad (2)$$

where x_1 and x_2 are the mole fractions of the end-members of the solution. The same cluster expansion has been successfully applied by Vinograd et al. (2007a) to model the effective pairwise interactions in the diopside–jadeite system. The J_n and A_i parameters were calculated by a least squares fit to 800 energy configurations selected according to the following scheme. Initial configurations were prepared from the supercell of $P2/n$ omphacite, CaMgNaAlSi$_4$O$_{12}$, where M21, M22, M11 and M12 sites are fully occupied by Ca, Mg, Na and Al, respectively. Firstly, Na was substituted for K and then appropriate numbers of Ca and Mg were substituted for K and Al so that after the substitution the mole fractions of K-Jd were 0.125, 0.25, 0.375, 0.5, 0.625, 0.75 and 0.875. Each of these configurations was subjected to 100 successive modifications obtained by subsequent swaps of atoms in a randomly chosen pairs of (K, Ca) or (Al, Mg). Additional 100 structures were prepared by random rearrangements from $P2/n$ omphacite in which K and Ca were
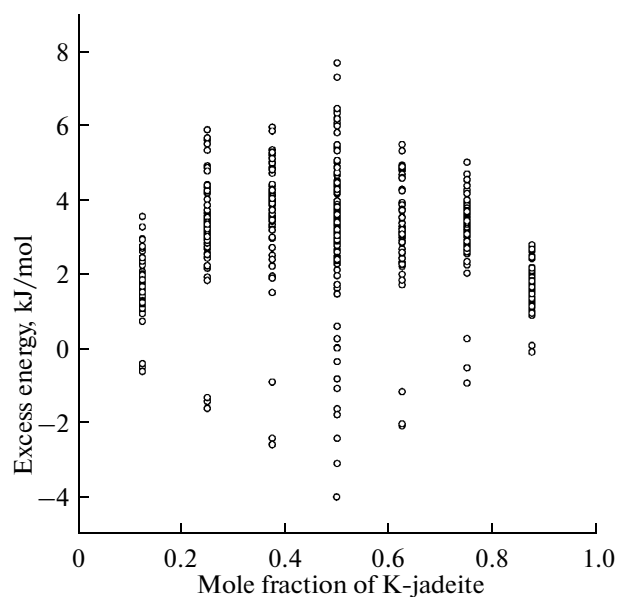
Fig. 1. Excess energies of configurations in $2 \times 2 \times 4$ supercell of diopside (circles) used for the calculation of effective pairwise energies (circles).

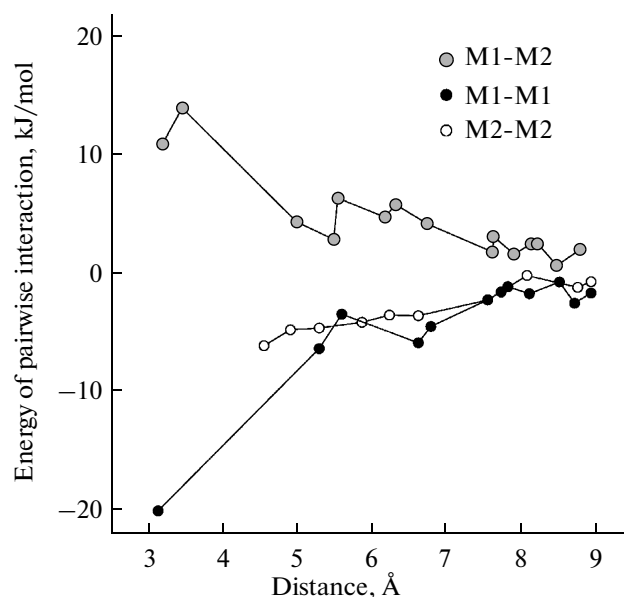All values correspond to a formula unit with 3 oxygens.

Fig. 2. Effective pairwise energies in the diopside−K-jadeite system as a function of the interatomic separation.

The distances are calculated for the diopside unit-cell with $a = 9.750$ Å, $b = 8.928$ Å, $c = 5.277$ Å and $\beta = 106.13°$ (Cameron et al., 1973).

completely rearranged (i.e., the cation in the M21 site was swapped with the cation in the M22 site). The static lattice energies of these configurations were calculated with GULP by minimizing the lattice energy with full relaxation of the structure. The excess ener-

Table 5. Parameters of cluster expansion

M1-M2		M2-M2		M1-M1	
d (Å)	J	d (Å)	J	d (Å)	J
3.191	10.875	4.555	−6.145	3.132	−20.076
3.455	13.900	4.908	−4.807	5.295	−6.389
4.494	4.281	5.295	−4.651	5.598	−3.491
5.488	2.820	5.868	−4.175	6.625	−5.910
5.544	6.294	6.237	−3.570	6.794	−4.525
6.177	4.701	6.625	−3.621	7.557	−2.285
6.322	5.756	7.557	−2.294	7.737	−1.609
6.749	4.117	8.083	−0.225	7.826	−1.167
7.626	1.743	8.764	−1.229	8.116	−1.759
7.634	3.052	8.943	−0.754	8.520	−0.772
7.912	1.573			8.723	−2.565
8.140	2.436			8.943	−1.697
8.233	2.410				
8.485	0.620				
7.799	1.967				

Note: The J values are in kJ/mol of M1 cations.

gies of these configurations are plotted in Fig. 1. The effective pairwise energies J_n obtained with the least square fit are plotted in Fig. 2 and listed in Table 5. The correlation coefficient is 0.993. The values for A_1 and A_2 parameters were −1.1393 and 0.1294 kJ/mol, respectively.

Figure 2 shows that the absolute values of effective pairwise energies rapidly decrease with the increase in the interatomic distance. This means that allowing for interactions of longer range than this covered by the $2 \times 2 \times 4$ supercell would not lead to a significant change of the partition function. This implies that the obtained expansion model (Equations 1 and 2) could be extrapolated to a much larger cell. Hence, the thermal average values of the functions of mixing can be calculated using a Monte Carlo algorithm. In this work, the Monte Carlo simulations were performed using an $8 \times 8 \times 12$ diopside supercell with periodic boundary conditions (6144 exchangeable sites). The average values were calculated by summation over successive enthalpy states produced in sufficiently long Monte Carlo runs. The conversion to the Boltzmann distribution was achieved through the application of the Metropolis algorithm (Metropolis et al., 1953). More detailed description of similar calculations using the Monte Carlo method was given in (Vinograd et al., 2007a). The main results are shown in Figs. 3−6. The local minima in the excess enthalpy of mixing at compositions 1/3, 5/12, 1/2, 7/12, and 2/3 (Fig. 3) correspond to the stabilization of intermediate compounds C_1, B_1, A_1, B_2, and C_2, respectively. The optimized cell
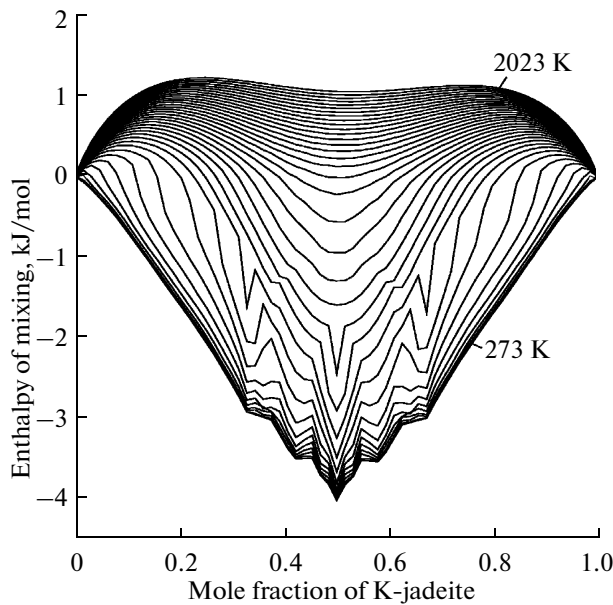
Fig. 3. Isotherms of the enthalpy of mixing of diopside–K-jadeite solid solution (solid lines) predicted using Monte Carlo simulations.

parameters of the C_1 and A_1 compounds are given in Table 2. The phase B_1 with the composition $x = 5/12$ has $P2/c$ space group with $a = 31.750$ Å, $b = 26.587$ Å, $c = 28.850$ Å, $\beta = 74.156°$. The structures of these compounds were determined from the Monte Carlo simulation at gradual decrease of temperature. The space groups of A, B, and C (Fig. 4), which recorded the low-temperature distribution of atoms, were determined using the "Materials Studio" package (http://accelrys.com/products/materials-studio). The Gibbs free energies (Fig. 5) were calculated from the average enthalpies using the method of thermodynamic integration (Myers et al., 1998; Warren et al., 2001). The application of the method to the diopside–jadeite solid solution was described by Vinograd et al. (2007a).

The obtained isotherms of free energies of mixing were used to calculate the $T–X$ phase diagrams (Fig. 6)
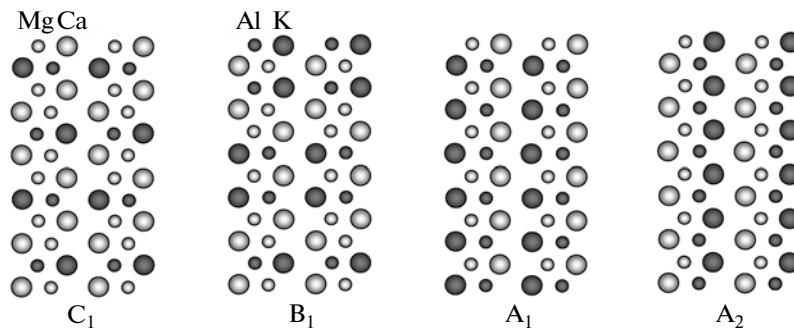
with a common tangent method. Phase diagram at low temperatures is characterized by several immiscibility gaps that are separated by narrow intervals of stability of intermediate compounds. The compounds B_2 and C_2 have the structures similar to those of the compounds B_1 and C_1, respectively, and can be obtained from the latters by substitution of Ca for K and Mg for Al.

Discrete values of free energy of mixing (G^{mix}) obtained by modeling are not suitable for petrological applications. Therefore, the excess free energies were fitted with a modified Guggenheim polynomial:

$$G_{excess} = x_1 x_2 \sum_{n=1}^{3} (A_n + TB_n)(x_2 - x_1)^{2n-2} + H_0, \quad (3)$$

where x_1 and x_2 are mole fractions of diopside and K-jadeite, respectively. Since the asymmetric component of the free energy of mixing is contained within H_0, it was convenient to subtract this term from the total energy of mixing and fit the rest with the symmetric Guggenheim polynomial containing $(x_2 - x_1)$ terms in even powers. Thus, for calculation of the total free energy of mixing, term H_0 must be added to the component described by equation 3 (the coefficients of polynomial are given in Table 6). At temperatures lower than 800°C the fitting with a polynomial is not possible because the free energy functions are strongly perturbed by the ordering. Therefore, the proposed model of mixing energy is applicable only within a range of 1073–1873 K. Since K-bearing clinopyroxenes occur only in the mineral assemblages that are formed at comparatively high temperatures, this range essentially covers possible applications.

DISCUSSION AND APPLICATIONS

Reasonable agreement between the estimates of excess enthalpies of intermediate compounds A_1, A_2, and C_1 in the $CaMgSi_2O_6–KAlSi_2O_6$ series calculated using GULP and CASTEP programs (Table 2) indicates that the force-field model is sufficiently accurate
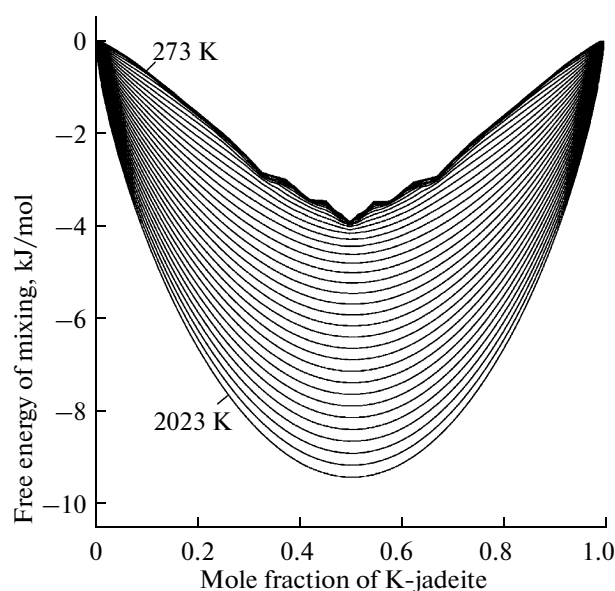

Fig. 4. The arrangement of cations within phases A_1, A_2, B_1, and C_1 along the chains parallel to the c-axis of the clinopyroxene structure.

Fig. 5. Gibbs free energy of mixing deduced from the thermodynamic integration.
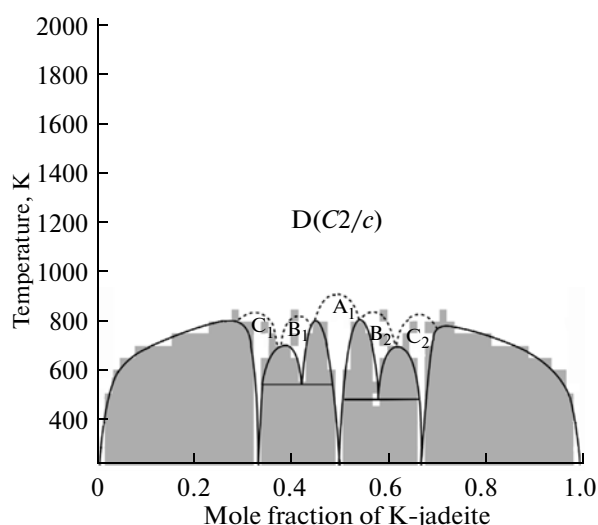

Fig. 6. The $T–X$ phase diagram constructed using results of Monte Carlo simulations and thermodynamic integration (solid lines). The dashed lines show an approximate location of the order/disorder transitions. The crystal structures of the ordered phases C_1 and A_2 are given in Table 2, whereas the arrangements of atoms in these structures are shown in Fig. 4. Their standard thermodynamic properties are given in Table 5.

to estimate the relative stability of intermediate compounds at relatively low pressures. Figure 6 shows that the mixing is complete at temperatures above 1000 K. However, already at 900 K, the model predicts phase transitions, which lead to the formation of omphacite-like phases. A scheme of ordering of K-omphacite A_1 differs from that of K-omphacite A_2, which is isostructural to Na-ompahcite. In A_1 structure, K and Ca are located in sites that would be occupied by Ca and Na, respectively, in Na-omphacite. The stability of A_1 structure in the K-bearing system and the inverse relationships between the energies of A_1 and A_2 in the Na-bearing system correlate with relative strength of M1–M2 interactions at the distances of 3.191 and 3.455 Å (Vinograd et al., 2007a). In the K-bearing system, the interaction at a distance of 3.191 Å is weaker

Table 6. Coefficients of the polynomial for the excess free energy in the diopside–K-*Jd* solid solution

N	A_n (J/mol)	B_n (J/mol K)
	1073–1873 K	
1	−2074.4	3.775
2	10879.7	−2.896
3	−662.6	1.468

Note: The Redlich-Kister term in Eqn. 1 describes the symmetric part of the excess free energy. The Margules polynomial with the parameters $A_{12} = −1.1393$ and $A_{21} = −0.1294$ kJ/mol must be added to get the total excess free energy.

than at 3.455 Å. Therefore, the formation of Ca–Al and Mg–K pairs in the K-bearing system requires less energy when they are arranged at the first-neighbor distance. On the contrary, the formation of Ca–Al and Mg–K pairs in the Na-bearing system requires less energy when they are arranged at the second-neighbor distance. The opposite relationships between A_1 and A_2 structures in the Na- and K-bearing systems indicate that the substitution of Na for K in the A_2 structure is not isostructural: an increase of K content leads to a phase transition, because K tends to substitute Ca, not Na. An increase of Na content in clinopyroxene reduces the number of sites, which can be substituted for K. Such crystal chemical a peculiarity could explain the negative correlation between Na and K, which is well known for omphacite inclusions in diamonds (e.g., Sobolev et al., 1998; Kaminsky et al., 2000; Pokhilenko et al., 2004) and synthetic K–Na-bearing clinopyroxenes (Safonov et al., 2004).

Our calculations show that in terms of unit-cell volume, K-jadeite is closer to diopside than to jadeite. This is consistent with significantly lower excess enthalpy estimated for the diopside–K-jadeite solid solution as compared to that of the diopside–jadeite system. Therefore, taking into account the calculated excess functions, we conclude that the diopside–K-jadeite solid solution at high temperature should be more ideal than the similar solution with jadeite. Moreover, the obtained $P–V$ data on diopside and K jadeite (Table 4) indicate that the volume difference between these end-members decreases with pressure. Thus, the mixing of these components at higher pres-

Table 7. Thermodynamic effects of selected mineral reactions involving K-jadeite at 298 K and 1 bar

Reaction number	Reaction	$\Delta H_{298,1}$, kJ/mol	$\Delta S_{298,1}$, J/K/mol	$\Delta V_{298,1}$, J/bar/mol
r1	K-*Jd* + *Coe* = *San*	−126.68	47.96	2.375
r2	K-*Jd* + *Sti* = *Hol*	4.88	0.46	−0.752
r3	K-*Jd* + *Coe* = KAlSi$_3$O$_8$ (melt)	−133.66	-39.04	2.856
r4	2K-*Jd* + *Coe* = Si-*Wd* + *Ky*	−123.41	11.22	0.236
r5	2K-*Jd* + *Sti* = Si-*Wd* + *Ky*	−153.25	27.52	0.899
r6	3K-*Jd* = Si-*Wd*+*Ky*+*Ks*	−217.95	44.78	1.861
r7	K-*Jd* = *Ks* + *Coe*	−94.54	33.56	1.625
r8	2K-*Jd* = *San* + *K*s	−221.22	81.52	3.982
r9	K-*Jd* = *Lc*	−96.34	58.76	2.349

Note: Thermodynamic parameters for K-*Jd* were obtained in this study. Thermodynamic data on *Coe*, *Ky*, *San* and KAlSi$_3$O$_8$ melt were taken from data base (Holland and Powell, 1998), while those on Si-*Wd* and *Hol* were taken from (Yong et al., 2006).

sures will be even closer to ideal. Therefore, it appears likely that the observed limited solubility of K-*Jd* in natural samples is caused not by immiscibility, but by the relatively high standard enthalpy of K-jadeite. Indeed, our quantum-mechanical calculations demonstrated that the sum of the standard enthalpies of K-jadeite and α-quartz is much higher than that of K-feldspar. This implies that K-*Cpx* can be in equilibrium with K-feldspar only when the mole fraction of K-*Jd* in solid solution is small. Similar conclusion follows for the SiO$_2$-undersaturated K-*Cpx* –leucite, kalsilite + coesite, kalsilite + sanidine, and Si-wadeite + kalsilite + kyanite assemblages (Liu, 1987). Indeed, the reactions K-*Jd* = *Lc*, 2K-*Jd* = *Ks* + *San*, K-*Jd* = *Ks* + *Coe*, and 3K-*Jd* = Si-*Wd* + *Ky* + *Ks* have large negative enthalpy effects and positive entropy effects (Table 7), what defines the instability of K-*Jd* in the abovementioned assemblages.

At the same time, large volume effect of the reaction K-*Jd* + *Qtz* = *Mic* (2.144 J/bar/mol) suggests that the pressure favors the stability of K-bearing clinopyroxene with respect to K-feldspar. When the mole fraction and the activity of K-*Jd* in the K-*Cpx* are known and KAlSi$_3$O$_8$ and SiO$_2$ polymorphs are present in the assemblage, the pressure can be estimated from the reaction:

$$\text{KAlSi}_2\text{O}_6 \text{ (in } Cpx) + \text{SiO}_2 = \text{KAlSi}_3\text{O}_8. \qquad (4)$$

The obtained thermodynamic parameters for K-*Jd* (Table 3) and parameters of the mixing model (Table 6) were used to calculate isopleths (lines of constant mole fractions of this component) of K-*Jd* in the binary *Di*−K-*Jd* solid solution in the assemblages of sanidine + coesite and hollandite + stishovite (Fig. 7). For the assemblages K-*Cpx* + *San* + *Coe* and K-*Cpx* + *Hol* + *Sti*, the isopleths were calculated from the equation

$$\Delta G = \Delta H - T\Delta S + \int_{298}^{T} \Delta C dT - T \int_{298}^{T} \frac{\Delta C}{T} dT$$
$$+ \int_{1}^{P} \Delta V dP + RT \ln K. \qquad (4)$$

In this equation, $\text{K} = 1/a_{\text{K-}Jd}^{\text{K-}Cpx}$ is the equilibrium constant, ΔH, ΔS, ΔV, and ΔC are the corresponding effects of reactions r1 and r2 (Table 7). The values of these effects were calculated using the obtained standard thermodynamic parameters for K-jadeite (Table 3) and standard thermodynamic functions of sanidine, coesite, stishovite (Holland and Powell, 1998) and hollandite (Yong et al., 2006). The activity of K-*Jd* end-member in the *Di*−K-*Jd* solid solution ($a_{\text{K-}Jd}^{\text{K-}Cpx}$) was calculated from equations (2) and (3) using data from Table 6. The temperature dependence of the heat capacity of K-jadeite was taken similar to that of diopside (Holland and Powell, 1998). As the transformation of sanidine into the hollandite structure at high pressure proceeds via the assemblage Si-*Wd* + *Ky* + *Coe* (Urakawa et al., 1994; Yagi et al., 1994; Fasshauer et al., 1998; Akaogi et al., 2004; Yong et al.,
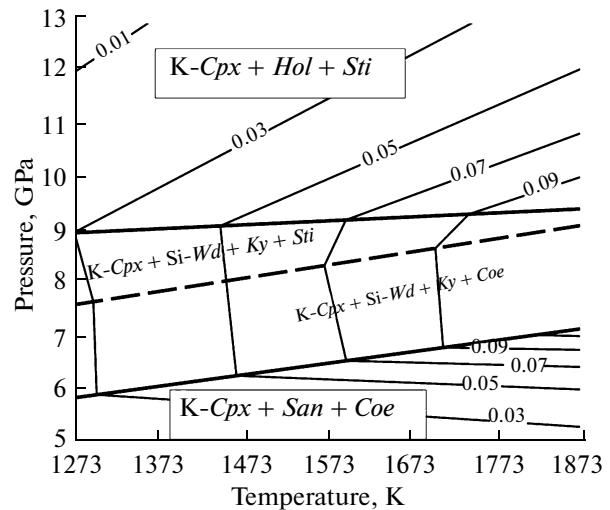

Fig. 7. Lines of constant mole fractions (isopleths) of K-*Jd* in clinopyroxene (thin lines) and the reaction boundaries (thick or dashed lines) for the assemblages in the silica-saturated system CaMgSi$_2$O$_6$−KAlSi$_3$O$_8$−SiO$_2$. The method of diagram calculation is explained in text.
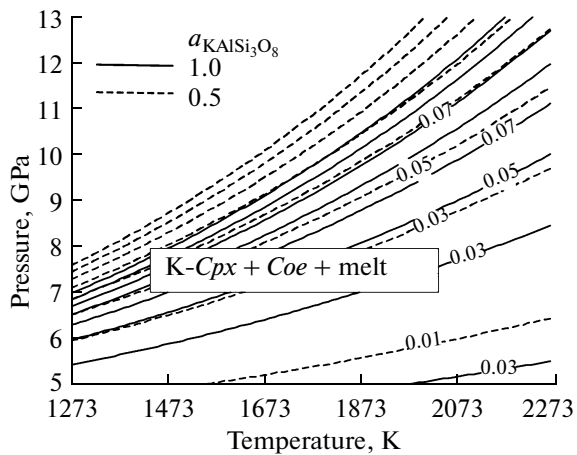
Fig. 8. Lines of constant mole fractions (isopleths) of K-*Jd* in clinopyroxene in the assemblage with coesite and aluminosilicate melt in the system $CaMgSi_2O_6$—$KAlSi_3O_8$—SiO_2 calculated for different activities of $KAlSi_3O_8$ in the melt $a_{KAlSi_3O_8}$ =1.0 (solid lines) and $a_{KAlSi_3O_8}$ = 0.5 (dashed lines).

2006), the isopleths of K-*Jd* were also calculated for the assemblages of Si-*Wd* + *Ky* + *Sti*/*Coe* using data on reactions r4 and r5 (Table 7). Si-*Wd*, *Ky*, *Coe*, and *Sti* were assumed to be phases of constant composition. The thermodynamic properties of kyanite, coesite, and stishovite were taken from the dataset of Holland and Powell (1998) and those of Si-wadeite, from the study of Yong et al. (2006).

The calculated diagram (Fig. 7) shows that the mole fraction of K-*Jd* in clinopyroxene in the presence of sanidine and coesite increases with pressure. However, an opposite tendency is observed in the assemblage with hollandite and stishovite. The slopes of the isopleths in hollandite and sanidine fields change consistently with the signs of volume and entropy effects of the reactions K-*Jd* + *Coe* = *San* and K-*Jd* + *St* = *Hol* (Table 7). These results are in qualitative agreement with the experiments on natural K-bearing basalt at pressures up to 15 GPa (Wang and Takahashi, 1999). These experiments demonstrate that the K_2O content in clinopyroxene in the *San* + *Coe* + *Grt* assemblage increases with pressure up to 6 GPa, and significantly decreases in the presence of hollandite and stishovite within the pressure range of 10–15 GPa. In all calculated assemblages, the mole fraction of K-*Jd* increases with temperature. The enrichment of clinopyroxene in potassium with increasing temperature was found in subsolidus experiments (Schmidt and Poli, 1998; Okamoto and Maruyama, 1998).

Figure 8 shows the isopleths of the K-*Jd* mole fraction in clinopyroxene in equilibrium with aluminosilicate melt and coesite, i.e., K-*Jd* + *Coe* = $KAlSi_3O_8$ (melt) (Table 7). The isopleths were obtained by calculating the equilibrium pressure from equation 4 written for the reaction r3 (Table 7) at independently vary-

ing values of $X_{K\text{-}Jd}^{Cpx}$ and T and at given activity of $KAlSi_3O_8$ ($a_{KAlSi_3O_8}$) in silicate melt. The value of reaction constant $K_{r3} = a_{KAlSi_3O_8}^{melt}/(a_{K\text{-}Jd}^{K\text{-}Cpx})$ were calculated using standard thermodynamic properties of $KAlSi_3O_8$ melt from the dataset (Holland and Powell, 1998). The positive slope of isopleths indicates that the mole fraction of K-*Jd* in clinopyroxene decreases with temperature. This effect is consistent with the experiments in the joins $CaMgSi_2O_6$–$KAlSi_2O_6$ and $CaMgSi_2O_6$–$KAlSi_3O_8$ (Safonov et al., 2003, 2005), which demonstrated a monotonous decrease of K-*Jd* content in clinopyroxene with temperature increase above the solidus. When $KAlSi_3O_8$ activity in the melt decreases, the isopleths are shifted toward the higher pressure fields, which is consistent with experimental data (see Perchuk et al., 2003 and Safonov et al., 2005 for review). The predicted range of K-*Jd* contents in clinopyroxenes is in good agreement with experiments. For instance, Fig. 8 demonstrates that the *Di*–K-*Jd* solid solution in equilibrium with K-rich aluminosilciate melt within the temperature range of 1000–1100°C and at pressure of 6 GPa contains 3–6 mol % K-*Jd*. Clinopyroxenes of similar compositions (5–8 mol % K-*Jd*) were synthesized in the $CaMgSi_2O_6$–$KAlSi_3O_8$ system at 6 GPa (Safonov et al., 2005).

It should be noted that the obtained model of K-*Cpx* solid solution permits only a qualitative interpretation of the abovementioned experimental data. The experiments correspond to systems, which have a more complex chemical and phase composition than this can be described with the present model. For instance, in the experiments of Wang and Takahashi (1999) and Schmidt and Poli (1998) K-bearing clinopyroxene, hollandite, and stishovite coexist with garnet, whereas clinopyroxene contains up to 60 vol % of jadeite. A more accurate description would require a clinopyroxene model which includes a wider range of end members. We hope that further simulation studies will make it possible to develop a thermodynamic model of the ternary diopside–jadeite–K-jadeite solid solution and to extend phase equilibrium calculations to chemically more complex systems.

REFERENCES

1. M. Akaogi, N. Kamii, A. Kishi, and H. Kojitani, "Calorimetric Study on High-Pressure Transition in $KAlSi_3O_8$," Phys. Chem. Minerals **31**, 85−91 (2004).

2. K. S. Aleksandrov, T. V. Ryzhova, and B. P. Belikov, "Elastic Properties of Pyroxenes," Sov. Fiz. Kristallografiya **8**, 589−591 (1964).

3. N. L. Allan, T. H. K. Barron, and J. A. O. Bruno, "The Zero Static Internal Stress Approximation in Lattice Dynamics, and the Calculation of Isotope Effects on Molar Volumes," J. Chem. Phys. **105**, 8300−8303 (1996).

4. U. Becker and K. Pollok, "Molecular Simulations of Interfacial and Thermodynamic Mixing Properties of Grossular-Andradite Garnets," Phys. Chem. Minerals **29**, 52−64 (2002).

5. U. Becker, A. Fernandez-Gonzalez, M. Prieto, et al., "Direct Calculation of Thermodynamic Mixing Properties of the Barite/Celestite Solid Solution from Molecular Principles," Phys. Chem. Minerals **27**, 291−300 (2000).

6. L. Bindi, O. G. Safonov, V. O. Yapaskurt, et al., "Ultrapotassic Clinopyroxene from the Kumdy-Kol Microdiamond Mine, Kokchetav Complex, Kazakhstan: Occurrence, Composition and Crystal-Chemical Characterization," Am. Mineral. **88**, 464−468 (2003).

7. L. Bindi, O. G. Safonov, Yu. A. Litvin, et al., "Ultrahigh Potassium Content in the Clinopyroxene Structure: An X-Ray Single-Crystal Study," Euro. J. Mineral. **14**, 929−934 (2002).

8. L. Bindi, R. T. Downs, G. E. Harlow, et al., "Compressibility of Synthetic Potassium-Rich Clinopyroxene: In Situ High-Pressure Single-Crystal X-Ray Study," Am. Mineral. **91**, 802−808 (2006).

9. F. C. Bishop, J. V. Smith, and J. B. Dawson, "Na, K, P and Ti in Garnet, Pyroxene, and Olivine from Peridotite and Eclogite Xenoliths from African Kimberlites," Lithos **11**, 155−173 (1978).

10. A. Bosenick, M. T. Dove, E. R. Myers, et al., "Computational Methods for the Study of Energies of Cation Distributions: Applications To Cation-Ordering Phase Transitions and Solid Solutions," Mineral. Mag. **65**, 193−219 (2001).

11. A. Bosenick, M. T. Dove, and C. A. Geiger, "Simulation Studies on the Pyrope-Grossular Solid Solution," Phys. Chem. Minerals **27**, 398−418 (2000).

12. M. Cameron, S. Sueno, C. T. Prewitt, and J. J. Papike, "High-Temperature Crystal Chemistry of Acmite, Diopside, Hedenbergite, Jadeite, Spodumene, and Ureyite," Am. Mineral. **58**, 594−618 (1973).

13. C. R. A. Catlow, "Computer Modeling of Silicates," in *Physical Properties and Thermodynamic Behavior of Minerals*, Ed. by E. K. H. Salje. NATO ASI Series **C225** (Reidel, Boston, 1988), pp. 619−638.

14. D. Cellai, T. M. Gesing, B. Wruck, and M. A. Carpenter, "X-Ray Study of the Trigonal-Hexagonal Phase Transition in Metamorphic Kalsilite," Am. Mineral. **84**, 1950−1955 (1999).

15. L. T. Chudinovskikh, V. A. Zharikov, R. A. Ishbulatov, and Yu. A. Matveev, "Mechanism of Ultrahigh Potassium Content Incorporation into High-Pressure Clinopyroxene," Dokl. Akad. Nauk **380** (6), 1−4 (2001) [Dokl. Earth Sci. **380**, 956−959 (2001)].

16. S. J. Clark, M. D. Segall, C. J. Pickard, et al., "First Principles Methods Using CASTEP," Zeitschrift für Kristallogr. **200**, 567−570 (2005).

17. J. W. D. Connolly and A. R. Williams, "Density-Functional Theory Applied To Phase Transformations in Transition-Metal Alloys," Phys. Rev. Bull. **27**, 5169−5172 (1983).

18. D. W. Fasshauer, B. Wunder, N. D. Chatterjee, and G. W. H. Höhne, "Heat Capacity of Wadeite-Type $K_2Si_4O_9$ and Pressure-Induced Stable Decomposition of K-Feldspar," Contrib. Mineral. Petrol. **131**, 210−218 (1998).

19. J. J. Finney and S. W. Bailey, "Crystal Structure of An Authigenic Maximum Microcline," Zeitschrift für Kristallogr. **119**, 413−436 (1964).

20. J. D. Gale and A. L. Rohl, "The General Utility Lattice Program (GULP)," Mol. Simulations **29**, 291−341 (2003).

21. J. D. Gale, "Analytical Free Energy Minimisation of Silicates," J. Phys. Chem. **102**, 5423−5431 (1998).

22. J. D. Gale, "Empirical Derivation of Interatomic Potentials for Ionic Materials," Philos. Mag. **73**, 3−19 (1996).

23. J. D. Gale, "GULP-a Computer Program for the Symmetry Adapted Simulation of Solids," J. Chem. Soc., Faraday Trans. **93**, 629−637 (1997).

24. M. R. Ghorbani and E. A. K. Middlemost, "Geochemistry of Pyroxene Inclusions from the Warrumbungle Volcano, New South Wales, Australia," Am. Mineral. **85**, 1349−1367 (2000).

25. G. E. Harlow and D. R. Veblen, "Potassium in Clinopyroxene Inclusions from Diamonds," Science **251**, 652−655 (1991).

26. G. E. Harlow, "Interpretation of KCpx and CaEs in Clinopyroxene from Diamond Inclusions and Mantle Samples," in *Proceedings of 7th International Kimberlite Conference, Cape Town, South Africa, 1999* (Cape Town, 1999), Vol. 1, 321−331 (1999).

27. G. E. Harlow, "K in Clinopyroxene at High Pressure and Temperature: An Experimental Study," Am. Mineral. **82**, 259−269 (1997).

28. R. F. S. Hearmon, *The Elastic Constants of Crystals and Other Anisotropic Materials*, Ed. by K. H. Hellwege and A.M. Hellwege, Landolt-Börnstein Tables, 1984, III/18 (Springer-Verlag, Berlin, 1984), pp. 1−154.

29. P. Hohenberg and W. Kohn, "Inhomogeneous Electron Gas," Phys. Rev. **136**, B864−B871 (1964).

30. T. J. B. Holland and R. Powell, "An Internally-Consistent Thermodynamic Dataset for Phases of Petrological Interest," J. Metamorph. Geol. **16**, 309−343 (1998).

31. A. L. Jaques, H. St. C. O' Neill, and C. B. Smith, "Diamondiferous Peridotite Xenoliths Form the Argyle

(AK1) Lamproite Pipe, Western Australia," Contrib. Mineral. Petrol. **104**, 255−276 (1990).

32. F. V. Kaminsky, O. D. Zakharchenko, and W. L. Griffin, D. M. Channer DeR., and G. K. Khachatryan-Blinova, "Diamond from the Guaniamo Area, Venezuela," Can. Mineral. **38**, 1347−1370 (2000).

33. A. V. Korsakov and J. Hermann, "Silicate and Carbonate Melt Inclusions Associated with Diamonds in Deeply Subducted Carbonate Rocks," Earth Planet. Sci. Lett. **241**, 104−118 (2006).

34. G. Kresse and J. Hafner, "Norm-Conserving and Ultrasoft Pseudopotentials for First-Row and Transition Elements," J. Physics: Cond. Matter **6**, 8245−8257 (1994).

35. M. Y. Lavrentiev, W. van Westrenen, N. L. Allan, et al., "Simulation of Thermodynamic Mixing Properties of Garnet Solid Solutions at High Temperatures and Pressures," Chem. Geol. **225**, 336−346 (2006).

36. L. Levien, C. T. Prewitt, and D. J. Weidner, "Structure and Elastic Properties of Quartz at Pressure," Am. Mineral. **65**, 920−930 (1980).

37. L. Liu, "High-Pressure Phase Transition of Potassium Aluminosilicates with Emphasis on Leucite," Contrib. Mineral. Petrol. **95**, 1−3 (1987).

38. T. Matsumoto, M. Tokonami, and N. Morimoto, "The Crystal Structure of Omphacite," Am. Mineral. **60**, 634−641 (1975).

39. N. Metropolis, A. Rosenbluth, M. Rosenbluth, et al., "Equation of State Calculations by Fast Computing Machines," J. Chem. Phys. **21**, 1087−1092 (1953).

40. H. O. A. Meyer, "Inclusions in Diamond," in *Mantle Xenoliths*, Ed. by P. H. Nixon (Wiley, Chichester, 1987), pp. 501−522.

41. E. R. Myers, V. Heine, and M. T. Dove, "Some Consequences of Al/Al Avoidance in the Ordering of Al/Si Tetrahedral Framework Structures," Phys. Chem. Minerals **25**, 457−464 (1998).

42. K. Okamoto and S. Maruyama, "Multi-Anvil Re-Equilibration Experiments of a Dabie Shan Ultra-High Pressure Eclogite within the Diamond-Stability Fields," Island Arcs **7**, 52−69 (1998).

43. S. Ono, J. P. Brodholt, and G. D. Price, "First-Principles Simulation of High-Pressure Polymorphs in $MgAl_2O_4$," Phys. Chem. Minerals **35**, 381−386 (2008).

44. E. J. Palin and R. J. Harrison, "A Monte Carlo Investigation of the Thermodynamics of Cation Ordering in 2−3 Spinels," Am. Mineral. **92**, 1334−1345 (2007).

45. A. Patel, G. D. Price, and M. J. Mendelsson, "A Computer-Simulation Approach To Modeling the Structure, Thermodynamics and Oxygen Isotope Equilibria of Silicates," Phys. Chem. Minerals **17**, 690−699 (1991).

46. L. L. Perchuk, O. G. Safonov, V. O. Yapaskurt, and J. M. Barton, "Jr. Crystal-Melt Equilibria Involving Potassium-Bearing Clinopyroxene As Indicators of Mantle-Derived Ultrahigh-Potassic Liquids: An Analytical Review," Lithos **60**, 89−111 (2002).

47. L. L. Perchuk, O. G. Safonov, V. O. Yapaskurt, and J. M. Barton, "Jr. Reply To Comments by Y. Zhu: K-Feldspar in Clinopyroxene from Grt-Cpx Silicate Rocks of the Kokchetav Massif," Lithos **68**, 121−130 (2003).

48. J. P. Perdew, K. Burke, and M. Ernzerhof, "Generalized Gradient Approximation Made Simple," Phys. Rev. Lett. **77**, 3865−3868 (1996).

49. N. P. Pokhilenko, N. V. Sobolev, V. N. Reutsky, et al., "Crystalline Inclusions and C-Isotope Ratios in Diamonds from the Snap Lake/King Lake Kimberlite Dyke System: Evidence of Ultradeep and Enriched Lithospheric Mantle," Lithos **77**, 57−67 (2004).

50. M. Prinz, D. V. Manson, P. F. Hlava, and K. Keil, "Inclusions in Diamonds: Garnet Lherzolite and Eclogite Assemblages," Phys. Chem. Earth **9**, 797−815 (1975).

51. M. Raudsepp, F. C. Hawthorne, and A. C. Turnock, "Crystal Chemistry of Synthetic Pyroxenes on the Join $CaNiSi_2O_6$−$CaMgSi_2O_6$ (Diopside): A Rietveld Refinement Study," Am. Mineral. **75**, 1274−1281 (1990).

52. A. M. Reid, R. W. Brown, J. B. Dawson, et al., "Garnet and Pyroxene Compositions in Some Diamondiferous Eclogites," Contrib. Mineral. Petrol. **58**, 203−220 (1976).

53. R. S. Ricard, J. W. Harris, J. J. Gurney, and P. Cardoso, "Mineral Inclusions in Diamonds from the Koffiefontein Mine," Geol. Soc. Austral. Spec. Publ. **14**, 1054−1062 (1989).

54. O. G. Safonov, L. L. Perchuk, Y. A. Litvin, and L. Bindi, "Phase Relations in the $CaMgSi_2O_6$−$KAlSi_3O_8$ Join at 6 and 3.5 GPa As a Model for Formation of Some Potassium-Bearing Deep-Seated Mineral Assemblages," Contrib. Mineral. Petrol. **149**, 316−337 (2005).

55. O. G. Safonov, L. L. Perchuk, and Yu. A. Litvin, "Equilibrium of Potassium-Bearing Clinopyroxene with Melt as Model for Barometry of Deep Associations," Geol. Geofiz. **46**, 1318−1334 (2005).

56. O. G. Safonov, L. L. Perchuk, and Yu. A. Litvin, "Effect of Carbonates on Crystallization and Composition of Potassium-Bearing Clinopyroxene at High Pressures," Dokl. Akad. Nauk **408** (2), 228−233 (2006) [Dokl. Earth Sci. **408**, 580−585 (2006)].

57. O. G. Safonov, Y. A. Litvin, L. L. Perchuk, et al., "Phase Relations of Potassium−Bearing Clinopyroxene in the System $CaMgSi_2O_6$−$KAlSi_2O_6$ at 7 GPa," Contrib. Mineral. Petrol. **146**, 120−133 (2003).

58. O. G. Safonov, Yu. A. Litvin, and L. L. Perchuk, "Synthesis of Omphacites and Isomorphic Features of Clinopyroxenes in the System $CaMgSi_2O_6$−$NaAlSi_2O_6$−$KAlSi_2O_6$," Petrologiya **12** (1), 84−97 (2004) [Petrology **12**, 70−81 (2004)].

59. J. M. Sanchez, F. Ducastelle, and D. Gratias, "Generalized Cluster Description of Multicomponent Systems," Phys. A **128A**, 334−350 (1984).

60. M. J. Sanders, M. Leslie, and C. R. Catlow, "Interatomic Potentials for SiO_2," J. Chem. Soc., Chem. Com. **19**, 1271−1273 (1984).

61. M. W. Schmidt and S. Poli, "Experimentally Based Water Budgets for Dehydrating Slabs and Consequences for Arc Magma Generation," Earth Planet. Sci. Lett. **163**, 361−379 (1998).

62. N. V. Sobolev and V. S. Shatsky, "Diamond Inclusions in Garnets from Metamorphic Rocks: a New Environ-

ment for Diamond Formation," Nature **343**, 742–746 (1990).

63. N. V. Sobolev, E. S. Yefimova, D. M. DeR. Channer, P. F. N. Anderson, and K. M. Barron, "Unusual Upper Mantle Beneath Guaniamo, Guyana Shield, Venezuela: Evidence from Diamond Inclusions," Geology **26**, 971–974 (1998).

64. T. Stachel, G. P. Brey, and J. W. Harris, "Kankan Diamonds (Guinea) I: from the Lithosphere Down To the Transition Zone," Contrib. Mineral. Petrol. **140**, 1–15 (2000).

65. D. K. Swanson and C. T. Prewitt, "The Crystal Structure of $K_2Si^{VI}Si^{IV}_3O_9$," Am. Mineral. **68**, 581–585 (1983).

66. S. Urakawa, T. Kondo, and N. Igawa, "Synchrotron Radiation Study on the High-Pressure and High-Temperature Phase Relations of $KAlSi_3O_8$," Phys. Chem. Minerals **21**, 387–391 (1994).

67. D. Vanderbilt, "Soft Self-Consistent Pseudopotentials in a Generalized Eigenvalue Formalism," Phys. Rev. **41**, 7894–7895 (1990).

68. V. L. Vinograd and M. H. F. Sluiter, "Thermodynamics of Mixing in Pyrope-Grossular, $Mg_3Al_2Si_3O_{12}$–$Ca_3Al_2Si_3O_{12}$, Solid Solution from Lattice Dynamics Calculations and Monte Carlo Simulations," Am. Mineral. **91**, 1815–1830 (2006).

69. V. L. Vinograd, B. P. Burton, J. D. Gale, et al., "Activity-Composition Relations in the System $CaCO_3$–$MgCO_3$ Predicted from Static Structure Energy Calculations and Monte Carlo Simulations," Geochim. Cosmochim. Acta **71**, 974–983 (2007b).

70. V. L. Vinograd, B. Winkler, A. Putnis, et al., "Thermodynamics of Pyrope-Majorite, $Mg_3Al_2Si_3O_{12}$–$Mg_4Si_4O_{12}$, Solid Solution from Atomistic Model Calculations," Mol. Simul. **32**, 85–99 (2006).

71. V. L. Vinograd, J. D. Gale, and B. Winkler, "Thermodynamics of Mixing in Diopside-Jadeite, $CaMgSi_2O_6$–$NaAlSi_2O_6$, Solid Solution from Static Lattice Energy Calculations," Phys. Chem. Minerals **34**, 713–725 (2007a).

72. V. L. Vinograd, L. L. Perchuk, T. V. Gerya, et al., "Order/Disorder Phase Transition in Cordierite and Its Possible Relationship to the Development of Symplectite Reaction Textures in Granulites," Petrologiya **15** (5), 459–473 (2007) [Petrology **15**, 427–440 (2007)].

73. W. Wang and E. Takahashi, "Subsolidus and Melting Experiments of a K-Rich Basaltic Composition to 27 GPa: Implication for Behavior of Potassium in the Mantle," Am. Mineral. **84**, 357–361 (1999).

74. M. C. Warren, M. T. Dove, E. R. Myers, et al., "Monte Carlo Methods for the Study of Cation Ordering in Minerals," Mineral. Mag. **65**, 221–248 (2001).

75. B. Winkler, M. T. Dove, and M. Leslie, "Static Lattice Energy Minimization and Lattice Dynamics Calculations on Aluminosilicate Minerals," Am. Mineral. **76**, 313–331 (1991).

76. A. Yagi, T. Suzuki, and M. Akaogi, "High-Pressure Transition in the System $KAlSi_3O_8$–$NaAlSi_3O_8$," Phys. Chem. Minerals **21**, 12–17 (1994).

77. W. Yong, E. Dachs, A. C. Withers, and E. J. Essene, "Heat Capacity and Phase Equilibria of Hollandite Polymorph of $KAlSi_3O_8$," Phys. Chem. Minerals **33**, 167–177 (2006).